applied optics

Quality assessment of refocus criteria for particle imaging in digital off-axis holography

Soumaya Kara Mohammed,[1,2,3] Larbi Bouamama,[2] Derradji Bahloul,[4] and Pascal Picart[3,5,*]

[1]Centre de Développement des Technologies Avancées (CDTA), Unité de Recherche en Optique et Photonique (UROP), Université Ferhat Abbas 1, Sétif 19000, Algeria
[2]Laboratoire d'Optique Appliquée, Institut d'Optique et Mécanique de Précision, Université Ferhat Abbas de Sétif, Sétif 19000, Algeria
[3]Université du Maine, CNRS UMR 6613, LAUM, Avenue Olivier Messiaen, 72085 Le Mans Cedex 9, France
[4]Département de Physique, Faculté des Sciences de la Matière, Université de Batna, Batna-1 05000, Algeria
[5]École Nationale Supérieure d'Ingénieurs du Mans, rue Aristote, 72085 Le Mans Cedex 9, France
*Corresponding author: pascal.picart@univ-lemans.fr

Received 1 December 2016; accepted 4 March 2017; posted 8 March 2017 (Doc. ID 281944); published 28 March 2017

This paper proposes a quality assessment of focusing criteria for imaging in digital off-axis holography. In the literature, several refocus criteria have been proposed in the past to get the best refocus distance in digital holography. As a general rule, the best focusing plane is determined by the reconstruction distance for which the criterion function presents a maximum or a minimum. To evaluate the robustness of these criteria, 13 criteria are compared with application on both amplitude and phase objects from off-axis holographic data. Simulation and experimental results lead to define a general rule and to exhibit the most robust criteria for accurate and rapid refocusing in digital holography.

OCIS codes: (090.1995) Digital holography; (090.2880) Holographic interferometry; (100.3175) Interferometric imaging; (110.3010) Image reconstruction techniques.

https://doi.org/10.1364/AO.56.00F158

1. INTRODUCTION

Digital holography (DH) and digital holographic microscopy (DHM) [1–3] are techniques for recording and reconstructing three-dimensional images of objects. In addition, digital holographic imaging is a very efficient technique for the measurement of deformation fields of the object surface and for the measurement of surface shapes and contours [4]. As a general rule, the object field is numerically reconstructed using a propagation operator (discrete Fresnel transform, angular spectrum [1–3]) in which an important parameter is the refocusing distance. Thus, an in-focus image can be obtained under the condition that the focusing distance is as close as possible to the exact optical path in the experimental setup. Therefore, a criterion to estimate if the reconstructed image is at the best focus has to be considered. Many refocus criteria have been proposed in past years. As a general rule, the best focusing plane is determined by the reconstruction distance for which the considered criterion function presents an extremum (maximum or minimum). Gillespie and co-workers [5,6] used self-entropy (ENTR) as a focus metric based on the phase distribution of the reconstructed hologram. Ma *et al.* [7] applied gray-level variance (VAR) on the intensity distribution of the reconstructed hologram at different depth planes. In the same way, Tachiki *et al.* [8] used gray-level VAR as a criterion in DH to determine the depth of multiple objects from a single hologram. Dubois *et al.* [9] proposed the integrated amplitude (Md) to determine the refocus distance of objects in DHM. This measure is similar to the L_1 norm. The measurement is based on the maximum of the scanning curve for Md image, while it is based on minimum for the phase one. Antkowiak *et al.* [10] exploited this work to create an extended focused image (EFI). The integrated modulus of amplitude is locally applied to create an image of the microscopic scene where all objects are in-focus. Note that a criterion similar to the L_2 norm (energy) was also proposed [11–13] and is close to the VAR criterion. The use of gradient (GRA) as a refocus criterion was discussed in [14]. Langehanenberg *et al.* and Toy *et al.* [15,16] reviewed the application of four focusing techniques [namely, GRA, Laplacian (LAP), VAR and logarithmically weighted Fourier spectral function (SPEC)] to phase and amplitude objects, and discussed in detail some of the important requirements for application in DHM. Yang and co-workers [17–19] discussed a focus measure called the correlation coefficient (CC) that was applied to particle image DH. They reconstructed holograms over a range of depths and created a sequence of these reconstructions in a volume. Then, the correlation between each of two images at the same distance as half of the correlation interval from that plane was calculated. The highest CC indicates the in-focus images. Grare *et al.* [20] used

Table 1. Focus Metrics and Their Application Domain

Criteria	Amplitude	Phase	Domain	Refs.
ENTR	×	×	DH	[5,6]
Md	×	×	DHM	[9,10]
GRA	×	×	DHM	[14,15,16]
LAP	×	×	DHM	[15,16]
VAR	×	×	DHM	[7,8,15,16]
SPEC	×	×	DH	[15,16,26]
CC	×		in-line DH	[17,18,19]
RC	complex field		in-line DH	[20]
TC	×	×	DH	[21,22]
GI	×			[23]

the complex ratio (RC), which is defined as the ratio between the VAR of the real part on the VAR of the imaginary part of the reconstructed image. This criterion was applied to digital in-line holography for particle imaging. Recently, two refocusing methods were discussed by Memmolo *et al.* [21,22] for both amplitude and phase objects: the Tamura coefficient (TC) and the Gini index (GI) [23]. Note that criteria were also discussed for application to multiwavelength DH [24,25]. Sparse representations can also be used to get refocus in DH [26]. Recently, Fonseca *et al.* demonstrated that normalized VAR, standard correlation, and GRA are the most reliable spatial-based metrics of the literature [27]. Table 1 summarizes the criteria from the literature with their application domain (DH, DHM, and in-line DH) on reconstructed object amplitude and/or reconstructed object phase.

Table 1 shows that these criteria were widely applied to amplitude and phase and that there is no rule to guide the choice for one or more of these criteria. It follows that a systematic approach for studying these criteria has to be implemented, in order to objectively compare them with the same set of data. In addition, such an approach has to test the criteria with both simulated and experimental data. Using simulated data is the most objective way to verify if the peak (or valley) of the metric is in good agreement with the exact best focus distance. Using experimental data is more powerful to test the robustness of the criteria according to noise and alias, which cannot be always perfectly simulated. So, in this paper, for holographic particle imaging, we aim at comparing the refocusing criteria summarized in Table 1 for amplitude and phase images obtained from off-axis holograms, on the one hand simulated and on the other hand experimentally recorded. This paper is organized as follows: Section 2 presents the metrics for each focusing criterion; Section 3 presents the principle of the simulation that was carried out to test the criteria; in Section 4, the results of the simulation for both amplitude and phase images of particles are presented. Section 5 provides the experimental setup and experimental results to perform the comparative study with opaque particles. In Section 6, discussion about the results is provided. Section 7 draws the conclusions to the study.

2. FOCUSING CRITERIA IN DH

As a general rule, the focusing metrics are evaluated on a selected part of the amplitude or phase of the reconstructed complex amplitude at a given reconstruction distance d_r. In this paper, we denote $A_z(k, l)$ as the amplitude of the complex field and $\varphi_z(k, l)$ its phase. The area on which criteria are evaluated includes $K \times L$ pixels. In order to generalize the application of the criteria, we note $\Psi(k, l)$ the data on which there are applied, i.e., amplitude, phase, or complex field. The metrics of each criterion are described hereafter. Entropy is defined as in Eq. (1) [5] by

$$\mathrm{ENTR} = -\sum_k p_k \log(p_k), \tag{1}$$

where p_k is the probability density function of Ψ in the selected area with $K \times L$ pixels. Dubois *et al.* [9] proposed a metric that is similar to L_1 norm and is defined as

$$M_d = \sum_k \sum_l |\Psi(k, l)|. \tag{2}$$

Langehanenberg *et al.* used four focus metrics to tackle the problem of autofocusing of reconstructed images of pure phase objects [15]. They considered GRA, LAP, VAR, and logarithmically weighted Fourier SPEC, whose metrics are, respectively, given by the following equations:

$$\mathrm{GRA} = \sum_k \sum_l \sqrt{(\Psi(k,l) - \Psi(k-1,l))^2 + (\Psi(k,l) - \Psi(k,l-1))^2}, \tag{3}$$

$$\mathrm{LAP} = \sum_k \sum_l \begin{pmatrix} \Psi(k+1, l) + \Psi(k-1, l) + \Psi(k, l+1) \\ +\Psi(k, l-1) - 4\Psi(k, l) \end{pmatrix}^2, \tag{4}$$

$$\mathrm{VAR} = \frac{1}{KL} \sum_k \sum_l (\Psi(k, l) - m_\Psi)^2, \tag{5}$$

$$\mathrm{SPEC} = \sum_u \sum_v \log(1 + F(u, v)\tilde{\Psi}(u, v)). \tag{6}$$

In Eq. (5), m_Ψ means average value of Ψ over the $K \times L$ pixels. In Eq. (6), $F(u, v)$ is a bandpass filtering applied to the Fourier transform of Ψ. For this criterion, we consider a high-pass filtering in the form of a circular binary mask, with radius R_u in the Fourier spectrum. Note that this criterion can be interpreted as a radial GRA metric, since the Fourier filtering selects high spatial frequencies as GRA filtering does. GRA and LAP metrics detect edges in digital images, and then the edge sharpness is greater when the reconstruction distance at the best focus plane is reached. Note that from the estimation of the VAR, the TC was used to refocus images with sparsity constraints [21]. The TC is defined as follows:

$$\mathrm{TC} = \sqrt{\frac{\sqrt{\mathrm{VAR}}}{m_Y}}. \tag{7}$$

In 2008, the CC was proposed for digital particle holography [17–19]. This metric measures the degree to which two images are similar. This coefficient metric calculates the ratio

between the CC between two images obtained at two different distances. Basically, it is computed according to Eq. (8), in which Ψ and Ψ' are data at the two considered distances:

$$\mathrm{CC} = \frac{\sum_k \sum_l (\Psi(k,l) - m_\Psi)(\Psi'(k,l) - m_{\Psi'})}{\sqrt{\sum_k \sum_l (\Psi(k,l) - m_\Psi)^2 \sum_k \sum_l (\Psi'(k,l) - m_{\Psi'})^2}}. \quad (8)$$

Another criterion proposed for digital particle holography was described by Grare *et al.* and is based on the ratio between the VAR of the real part and that of the imaginary part of the reconstructed complex field [20]:

$$\mathrm{RC} = \frac{\mathrm{VAR}[R_e(\Psi)]}{\mathrm{VAR}[I_m(\Psi)]}, \quad (9)$$

where VAR[…] is given by Eq. (5), R_e and I_m are, respectively, the real and imaginary part of Ψ (when data Ψ are complex valued, i.e., $\Psi = A_r \exp(i\varphi_r)$). It follows that this criterion is applied by considering the complex amplitude instead of the amplitude or the phase of the reconstructed image at distance d_r. In 2014, Memmolo *et al.* [22] used the GI to evaluate refocusing image with sparsity constraints. The GI is given by

$$\mathrm{GI} = 1 - \frac{2}{\|\Psi\|_1} \sum_n \left(\frac{N - n + 0.5}{N}\right) \Psi_{kl}(n), \quad (10)$$

where $\|\ldots\|_1$ is the L_1 norm, n varies from 1 to $K \times L$, and $\Psi_{kl}(n)$ are the sorted entries of $\Psi(k,l)$ in ascending order. The GI is well known to be a quasi-convex function, and it assumes values between 0 and 1.

In this paper, three more criteria are added for comparison: the average horizontal gradient (GRAX), the average vertical gradient (GRAY), and the maximum of the LAP in the selected area (LAPMAX). The GRAX and GRAY can be obtained by convoluting the data with GRA masks. This can be formalized according to Eq. (11), where "D" means "X" or "Y"; $*$ means convolution:

$$\mathrm{GRAD} = \Psi * P_D \quad (11)$$

and the GRA masks are defined as

$$P_X = \begin{bmatrix} 1 & 1 & 1 \\ 0 & 0 & 0 \\ -1 & -1 & -1 \end{bmatrix} P_Y = \begin{bmatrix} 1 & 0 & -1 \\ 1 & 0 & -1 \\ 1 & 0 & -1 \end{bmatrix}. \quad (12)$$

Criterion LAPMAX is calculated as

$$\mathrm{LAPMAX} = \max[\Psi * P_{XY}], \quad (13)$$

with the LAP mask

$$P_{XY} = \begin{bmatrix} -1 & -1 & -1 \\ -1 & 8 & -1 \\ -1 & -1 & -1 \end{bmatrix}. \quad (14)$$

In order to get a systematic approach for qualitatively appraising these refocus criteria, a full numerical simulation of the recording/reconstruction holographic process for particles was carried out. The next section describes the simulation.

3. SIMULATION OF THE HOLOGRAPHIC PROCESS

The numerical simulation was developed by taking into account the full acquisition and reconstruction process, including the particle, optical-wave propagation, interference pattern, recording and processing, and the final quantitative evaluation of each criterion. We choose to simulate off-axis DH for particle imaging that can be opaque or phase particle. The first part of the full simulation deals with the optical-wave propagation (diffraction, interferences), and the recording process (sensor with spatial rate, digitization with eight bits and photon noise). The second part deals with the reconstruction process, in which the reconstruction distance is varied, and criteria are applied for each distance. For both diffraction processes at recording and reconstruction, the angular spectrum transfer function is used, and convolution is calculated with the double fast Fourier transform (FFT) algorithm [2]. The wavelength is set at $\lambda = 457$ nm; the pixel pitches in the sensor and object plane are set to $p_x = p_y = 10$ μm. The sensor and object plane include 1024 pixels × 1024 pixels. After recovering the complex image field from the digital hologram, amplitude and phase are extracted, and criteria are systematically applied both on amplitude and phase.

A. Recording Process

Let $E(x,y)$ be the amplitude distribution of a particle with diameter φ_p illuminated by a plane wave, and located at distance d_0 from the sensor, as shown in Fig. 1. In what follows, it is considered that the object field propagates through a distance d_0, and interferes with a reference wave noted R to produce the hologram H. From the Huygens–Fresnel integral, the complex Md in the detector plane can be expressed as follows [1–4]:

$$O(x,y,d_0) = \frac{i}{\lambda d_0} \exp\left(\frac{2i\pi d_0}{\lambda}\right) \int_{-\infty}^{+\infty} \int_{-\infty}^{+\infty} E(x',y') w(x',y') \times \exp\left[\frac{i\pi}{\lambda d_0}((x'-x)^2 + (y'-y)^2)\right] \mathrm{d}x' \mathrm{d}y', \quad (15)$$

where $I = \sqrt{-1}$, λ is the wavelength of light, and $w(x,y)$ is the illuminating wavefront. This equation is numerically calculated

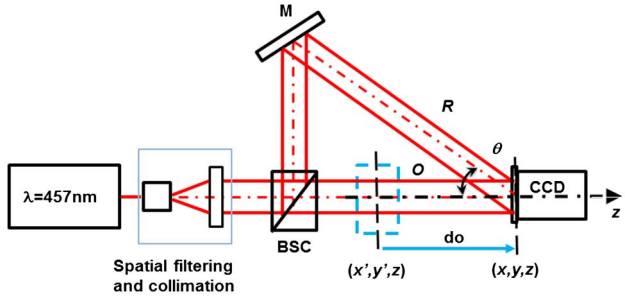

Fig. 1. Configuration for off-axis recording with a single beam to produce both reference and object wave (M, mirror; BSC, beam splitter cube); angle θ is related to the spatial frequencies u_0 and v_0 in Eq. (18); (x',y',z), set of reference axis attached to the object plane; (x,y,z), set of reference axis attached to the sensor plane.

using the convolution theorem and the angular spectrum transfer function in the Fresnel approximation. Thus, the complex amplitude in the detector plane can be computed according to [2–4,28]

$$O = \mathrm{FT}^{-1}[\mathrm{FT}[E] \times G], \tag{16}$$

where the transfer function G is given by Eq. (17):

$$G(u, v, d_0) = \exp(-i\pi\lambda d_0(u^2 + v^2)). \tag{17}$$

In the off-axis configuration, the reference wave is written as

$$R(x, y) = w(x, y)\exp(2i\pi(u_0 x + v_0 y)), \tag{18}$$

where u_0 and v_0 are the spatial frequencies of the reference wave. In the recording plane, the hologram is expressed as

$$H = |O|^2 + |R|^2 + OR^* + O^* R. \tag{19}$$

In order to get a more realistic simulation, we considered that the illuminating wave $w(x, y)$ producing object and reference waves (see Fig. 1), has Gaussian amplitude (TEM00 mode) with few diffraction patterns as pollution from reflection/transmission through optics. In addition, the digital holograms were recoded with an 8-bit sensor, and we took into account the photon noise. by considering that the pixel well includes 16,000 electrons at saturation.

B. Reconstruction Process

At any distance d_r the reconstruction of the complex amplitude of the object field is based on the convolution formulae of diffraction, similarto Eq. (16), with input data being H. The processing is as follows: first compute the Fourier transform of the hologram and select the +1 order by windowed filtering, get the +1 order at the sensor plane by calculating the inverse Fourier transform, then remove the spatial carrier frequency by multiplying by the complex conjugate of the phase term in Eq. (18). From the +1 order at the sensor plane, the image plane is obtained with Eq. (16) at any distance d_r, and the refocus criteria can be applied on amplitude $A_r(k, l)$ and phase $\varphi_r(k, l)$ of the calculated complex field.

C. Illustrations from Simulation

The simulation was performed with a single particle $\varphi_p =$ 40 μm in diameter. The initial position of the particle and the spurious diffraction pattern were randomly selected. The distance for the particle was found to be $d_0 = 80.91$ mm. The particle was chosen to be completely opaque or to be a pure phase object.

For testing the refocusing criteria, the region of interest (ROI) was chosen to be 10 times the diameter of the particle. This means that for this study, the ROI is 41 pixels × 41 pixels around the image of the particle.

Figure 2 shows images from the simulation. The illuminating Gaussian amplitude with random spurious patterns is shown in Fig. 2(a). Figures 2(b) and 2(c) show, respectively, the digital hologram and reconstructed image for an opaque particle. Figures 2(d) and 2(e) show, respectively, the digital hologram for a pure phase-object particle and the reconstructed phase image. Figure 2(f) shows a zoom of the ROI for the case of the reconstructed amplitude of the opaque particle.

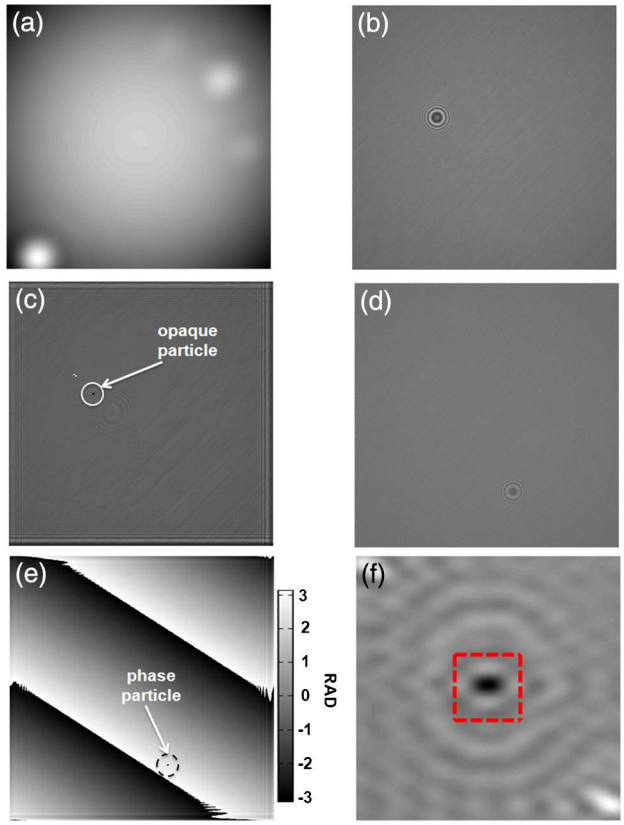

Fig. 2. Images from simulation. (a) Gaussian amplitude with random spurious patterns; (b) digital hologram for an opaque particle; (c) reconstructed amplitude image for an opaque particle; (d) digital hologram for a pure phase-object particle; (e) reconstructed phase image; (f) zoom of the ROI for the case of the opaque particle.

4. SIMULATION RESULTS

This section presents the results obtained with the simulation with both the holograms of the opaque particle and phase-object particle. For better readability of the curves, criteria are normalized between 0 and 1. The scanning distance range was chosen to be $d_r = \{d_0 - 40$ mm, $d_0 + 40$ mm$\}$ with steps of 0.4 mm.

A. Refocusing for an Opaque Particle

1. Refocusing Criteria Applied to the Reconstructed Md

Figures 3(a)–3(d) plot the criteria versus the reconstruction distance when applied on the reconstructed amplitude A_r from the reconstructed field with the opaque particle. Figure 3(a) shows criteria VAR, LAP, LAPMAX, GRA, GRAX, and GRAY. Curves exhibit a nice bell curve with a peak localized at reconstruction distance $d_r = 80.91$ mm; Fig 3(b) plots criteria SPEC, ENTR, GI, Md, TC, and RC, whereas Fig. 3(c) shows the CC criterion. Note that RC was calculated using the real and imaginary part of the reconstructed complex field, according to Eq. (9). Figure 3(d) exhibits the SPEC criterion when varying the reconstruction distance and the filtering radius in the Fourier spectrum. Values for R_u varied from 1% to 50% of the spatial cutoff frequency, which is equal to $1/2p_x$.

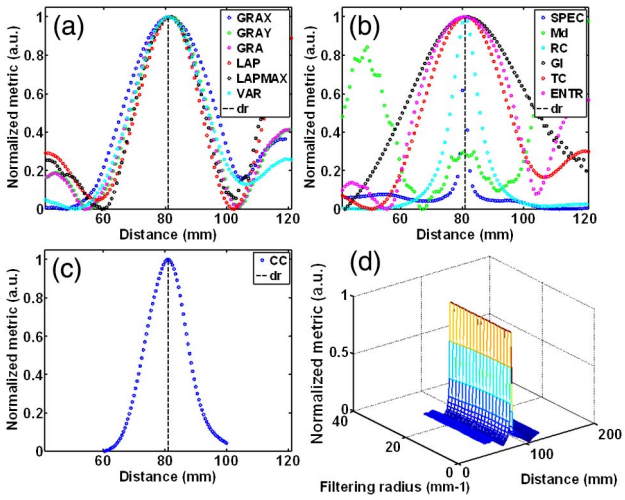

Fig. 3. Comparison of refocusing criteria versus reconstruction distance for opaque object, applied to the reconstructed amplitude. (a) Criteria VAR, LAP, LAPMAX, GRA, GRAX, and GRAY; (b) criteria SPEC, ENTR, GI, Md, TC, and RC; (c) criterion CC; (d) SPEC criterion when varying the reconstruction distance and the filtering radius in the Fourier spectrum.

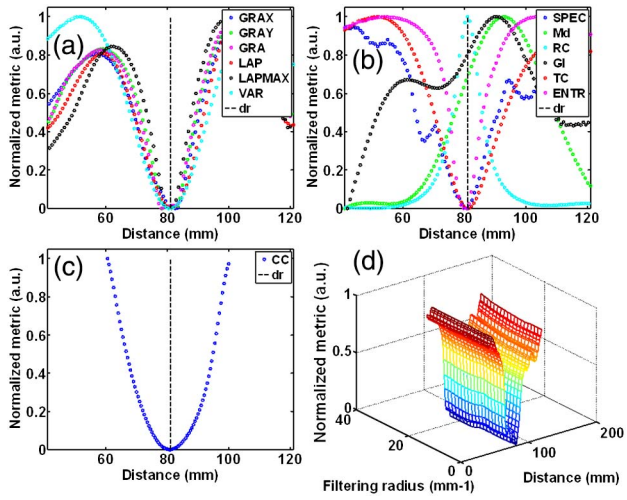

Fig. 4. Comparison of refocusing criteria versus reconstruction distance for opaque object, applied to the reconstructed phase. (a) Criteria VAR, LAP, LAPMAX, GRA, GRAX, and GRAY; (b) criteria SPEC, ENTR, GI, Md, TC, and RC; (c) criterion CC; (d) SPEC criterion when varying the reconstruction distance and the filtering radius in the Fourier spectrum.

Figures 3(b) and 3(c) show that criteria SPEC, ENTR, GI, TC, RC, and CC are able to produce a bell curve with a peak localized at reconstruction distance $d_r = 80.91$ mm, which is the theoretical simulated distance. Note that the curve obtained with SPEC is very narrow and looks more like a Dirac delta function rather than a bell curve. The Md criterion exhibits a minimum that is not localized at $d_r = 80.91$ mm, and the curve is not regular compared to others. We have no explanation for this behavior, but it seems to be correlated with Fig. 5 in [9].

The simulation shows that photon noise, quantization noise, and Gaussian illumination with few spurious patterns do not disturb the criteria, thus confirming their robustness. Figure 3(d) shows that SPEC is not sensitive to the choice of the filtering radius, since a peak is always reached at the good reconstruction distance, and the obtained curve always remains highly contrasted.

2. Refocusing Criteria Applied to the Reconstructed Phase

In the same way as in the previous section, the criteria were applied to the wrapped phase φ_r extracted from the reconstructed field with the opaque particle as the initial object.

Figure 4(a) shows criteria VAR, LAP, LAPMAX, GRA, GRAX, and GRAY. Figure 4(b) plots criteria SPEC, ENTR, GI, Md, TC, and RC, whereas Fig. 4(c) shows the CC criterion. Figure 4(d) exhibits the SPEC criterion when varying the reconstruction distance and the filtering radius in the Fourier spectrum.

Similar to Fig. 3(d), SPEC is not sensitive to the choice of the filtering radius. In Fig. 4(b), GI and Md do not provide a curve having a peak at the theoretical distance. For the other cases, curves exhibit a reverse bell curve showing a clear valley, as was found in the literature when applying criteria to the phase. Note that the bell-type curves are highly contrasted.

B. Refocusing for a Phase-Object Particle

1. Refocusing Criteria Applied to the Reconstructed Md

In this section, refocusing criteria are applied to the amplitude image obtained from the pure phase-object particle hologram. Figures 5(a)–5(d) plot the criteria versus the reconstruction distance. Figure 5(a) shows criteria VAR, LAP, LAPMAX, GRA, GRAX, and GRAY. Figure 5(b) plots criteria SPEC, ENTR, GI, Md, TC, and RC, whereas Fig. 5(c) shows the CC criterion. Figure 5(d) exhibits the SPEC criterion when varying the reconstruction distance and the filtering radius in the Fourier spectrum. Figure 5(a) shows a minimum peak for

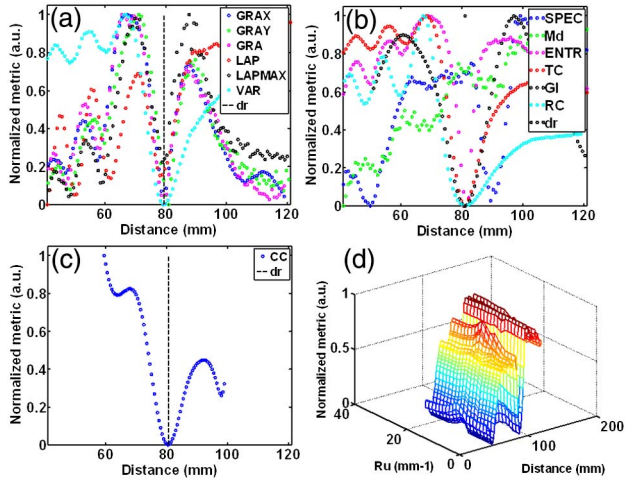

Fig. 5. Comparison of refocusing criteria versus reconstruction distance for phase-object particle, applied to the reconstructed Md. (a) Criteria VAR, LAP, LAPMAX, GRA, GRAX, and GRAY; (b) criteria SPEC, ENTR, GI, Md, TC, and RC; (c) criterion CC; (d) SPEC criterion when varying the reconstruction distance and the filtering radius in the Fourier spectrum.

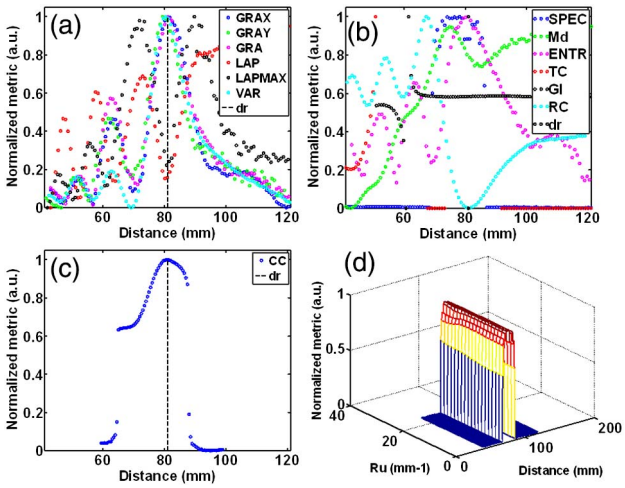

Fig. 6. Comparison of refocusing criteria versus reconstruction distance for phase-object particle, applied to the reconstructed phase. (a) Criteria VAR, LAP, LAPMAX, GRA, GRAX, and GRAY; (b) criteria SPEC, ENTR, GI, Md, TC, and RC; (c) criterion CC; (d) SPEC criterion when varying the reconstruction distance and the filtering radius in the Fourier spectrum.

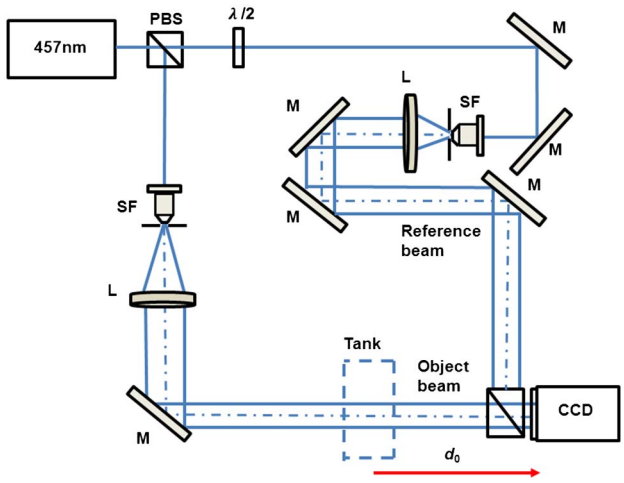

Fig. 7. Experimental setup. PBS, polarized beam splitter; SF, spatial filter; L, collimating lens; M, mirrors; CCD, recording sensor; $\lambda/2$: half-wave plate.

all criteria when the focus plane is reached at a distance of 80.91 mm. Figures 5(b) and 5(c) also shows a minimum peak for the same value of the reconstruction distance for the criteria ENTR, TC, and RC. However, SPEC, Md, and GI do not show such a peak at the theoretical distance. Figure 5(d) shows that there is no optimum choice for the filtering radius for the SPEC criterion that fails to give the correct focus distance, in this case.

2. Refocusing Criteria Applied to the Reconstructed Phase

In this section, refocusing criteria are applied to the modulo 2π phase image obtained from the pure phase-object particle hologram. Figures 6(a)–6(d) plot the criteria versus the reconstructing distance. Figure 6(a) shows criteria VAR, LAP, LAPMAX, GRA, GRAX, and GRAY. Figure 6(b) plots criteria SPEC, ENTR, GI, Md, TC, and RC, whereas Fig. 6(c) shows the CC criterion. Figure 6(d) exhibits the SPEC criterion when varying the reconstruction distance and the filtering radius in the Fourier spectrum.

For this case, there are no curves exhibiting regular and symmetric shape such as bell-type ones, but the large majority has the peak or the valley at the correct focus distance. Only TC, GI, and Md do not exhibit such a feature. Surprisingly, Md fails in this case, but it was developed for quantitative phase imaging in DHM. The reason for this behavior in this paper is certainly due to the fact that it is here applied on the wrapped phase. In related papers, it is generally applied to the unwrapped phase. Unfortunately, the phase image of the particle cannot be unwrapped.

5. EXPERIMENTAL RESULTS

A. Experimental Setup

In order to get a complementary overview on how the criteria may provide accurate focus distance, the criteria were applied on experimental phase and amplitude images obtained from experimental digital holograms of particles. The experimental setup is described in Fig. 7. A laser at $\lambda = 457$ nm is separated using a polarizing beam splitter to produce the reference and object beams. Both beams are expanded with spatial filtering and a collimating lens. The reference beam impacts the sensor with an incident angle producing an off-axis recording (see Fig. 1). The object beam crosses the particle plane. The sensor includes 1024 pixels × 1344 pixels with pixel pitches at 6.45 μm. At any reconstruction distance, the complex image is reconstructed using the convolution formulae of Eq. (16) with the +1 order as input data. Then, from the complex field, the amplitude image and phase image are computed and refocus criteria are calculated. The scanning distance range was chosen to $d_r = \{d_0 - 80\ \text{mm}, d_0 + 80\ \text{mm}\}$, with steps of 0.8 mm.

The object is a noncalibrated opaque particle with average diameter at about 150 μm (equivalent to about 32 pixels in the reconstructed plane). The particle falls in free fall in a quartz tank, with volume 1 cm × 1 cm × 4.5 cm, and filled with water. The particle in the tank is at about 300 mm from the sensor. The ROI for applying criteria is ±40 pixels around the center of the particle, such that it completely covers the surface occupied by the image of the particle. This was chosen so that the ROI encompasses the particle. If the ROI is too close to the particle, the criteria are not relevant and they are spread out. If the ROI is too large, then they become strongly irregular, exhibiting nonunderstood rapid variations versus distance scan. Before recording any digital hologram, a reference hologram without any particle in the optical path is recorded.

Digital holograms are processed as follows: the hologram is Fourier transformed and filtered to get the +1 order at the sensor plane; demodulation is carried out similar to simulations (see Section 3). Then, the complex field at the sensor plane is propagated along the reconstruction distance by convolution with the angular spectrum transfer function. The amplitude image is systematically divided by that obtained from the reference hologram. The reference phase image is systematically subtracted from the reconstructed object phase. Figure 8 shows the results obtained from the particle. Figure 8(a) shows the digital hologram of the

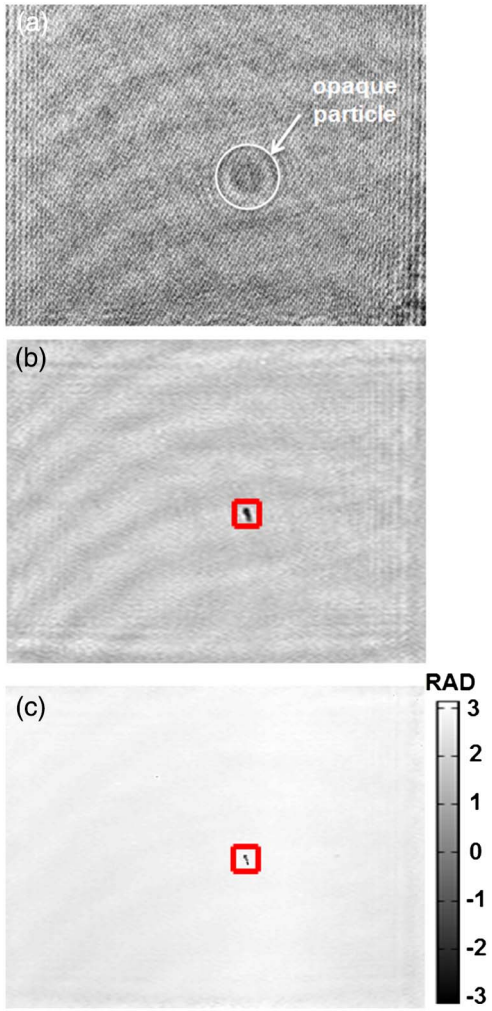

Fig. 8. Experimental results. (a) Digital hologram of particle; (b) reconstructed amplitude at distance 300 mm; (c) reconstructed phase image with ROI indicated with the red line and occupying 80 pixels × 80 pixels.

particle, and Fig. 8(b) exhibits the reconstructed amplitude at distance 300 mm. Figure 8(c) shows the reconstructed phase images. The ROI (80 pixels × 80 pixels) for application of refocus criteria is indicated with the red line in Figs. 8(b) and 8(c).

B. Refocusing Applied to Reconstructed Md Images

Following the approach of Section 4, the criteria were applied to the reconstructed amplitude images. Figures 9(a)–9(d) plot the criteria versus the reconstructing distance for the amplitude image. Figure 9(a) plots VAR, LAP, LAPMAX, GRA, GRAX, and GRAY. Figure 9(b) plots SPEC, ENTR, GI, Md, TC, and RC, and Fig. 9(c) plots CC, whereas in Fig. 9(d) SPEC is plotted versus distance and filtering radius in the Fourier spectrum. There are criteria exhibiting a maximum or minimum at the probable correct distance at about 300 mm, except ENTR. Criteria VAR, GRA, GRAX, GRAY, LAP, LAPMAX, TC, RC, SPEC, and CC produce a maximum peak at distance 300 mm. One can observe that Md and GI produce a minimum valley. However, only VAR, TC, RC, and Md exhibit a very regular bell-type curve, with a highly contrasted peak or valley.

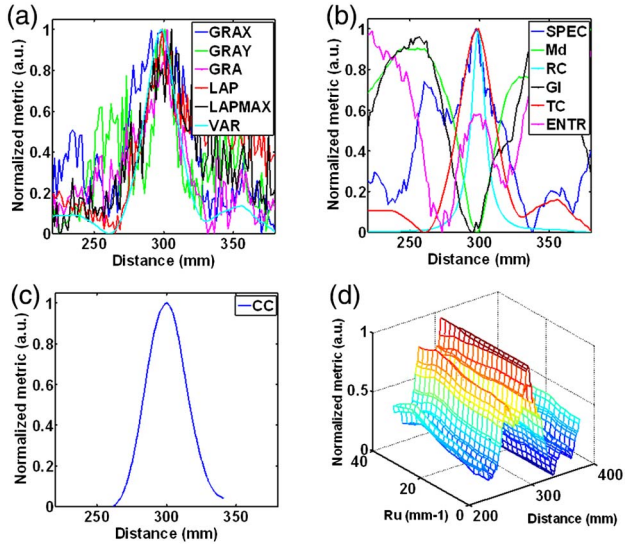

Fig. 9. Comparison of refocusing criteria versus reconstruction distance for particle reconstructed amplitude. (a) Criteria VAR, LAP, LAPMAX, GRA, GRAX, and GRAY; (b) criteria SPEC, ENTR, GI, Md, TC, and RC; (c) criterion CC; (d) SPEC criterion when varying the reconstruction distance and the filtering radius in the Fourier spectrum.

The other criteria exhibit a nonsymmetric and nonregular curve, but the maximum is in coincidence with the other maxima. Surprisingly, and this is unexplained, the ENTR criterion exhibits a secondary peak at the correct distance.

C. Refocusing Applied to Reconstructed Phase Images

In the same way as for the previous section, this section shows the results obtained with application of criteria to the reconstructed phase images of the particle [see Fig. 8(c)]. Note that strictly speaking the real object being an opaque object (opaque particle), the phase image would be irrelevant to apply any criteria. However, there do exist sharp transitions at the border between air and object in the phase, even if the particle completely blocks light [see Figs. 8(b) and 8(c)]. So, such sharp transitions are of interest to test the criteria. Figures 10(a)–10(d) shows the selected criteria.

Figure 10 shows that criteria VAR, LAP, CC, RC, ENTR, Md, and SPEC exhibit a significant peak (VAR, LAP, RC, SPEC) or valley (ENTR, CC, Md) at the probable focus distance. The other criteria fail to produce any peak or valley. In addition, Figs. 9(d) and 10(d) show that SPEC is not influenced by the filtering parameters when varying the filtering radius R_u from 1% to 50% of the spatial cutoff frequency (see Section 4.A). Note that CC, RC, and ENTR exhibit a very regular curve, whereas it is not the case for the other criteria, since they look more fluctuating.

The ENTR criterion seems to be more robust with the phase image than with the amplitude image.

D. Comparison of Computation Time

The computation cost of the criteria was evaluated with MATLAB on a laptop equipped with Intel Core i7-2600 3.40 GHz with 8 GB RAM. The computation times were

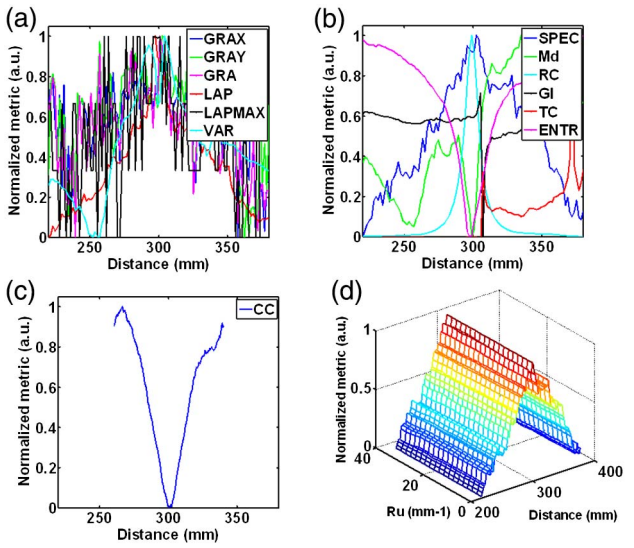

Fig. 10. Comparison of refocusing criteria versus reconstruction distance for particle reconstructed phase. (a) Criteria VAR, LAP, LAPMAX, GRA, GRAX, and GRAY; (b) criteria SPEC, ENTR, GI, Md, TC, and RC; (c) criterion CC; (d) SPEC criterion when varying the reconstruction distance and the filtering radius in the Fourier spectrum.

estimated as an average time for the calculation of 80 values for 80 reconstruction distances. Table 2 provides the estimated average computation times given in milliseconds. The SPEC is the longest one, because it requires filtering in the Fourier spectrum and thus requires FFT computation. Then, CC also is longer than the other ones, since it is based on computation of a CC. All other average values are in the range of few tens or hundreds of microseconds. Of course, such results do not prevent optimized computation, such as with GPU for example, which would be quite a bit faster. Table 2 provides a relative ranking according to the computation costs.

6. DISCUSSION

Results obtained through Section 4 with simulation and Section 5 permit us to draw a few general rules, although it is not so easy to provide systematic rules for applying the refocus criteria studied in this paper. First of all, many of the refocus criteria are able to produce a peak or a valley when the distance by considering a reconstructed amplitude image is scanned. This is demonstrated both with simulation results and experimental results with the particle. For the phase images obtained from phase particle, simulation shows that VAR and CC are the most robust criteria that can yield the correct distance. For the phase images obtained from experiment with a particle, few criteria produce a regular curve with a peak or a valley: CC, RC, and ENTR. Surprisingly, ENTR does produce such a regular curve for the phase image, whereas it does not for the amplitude image [see Fig. 9(b)]. The reasons for such results are not clear. The more robust criterion with experimental data is CC because it provides regular and very well-contrasted curves (peak or valley) with both amplitude and phase. The reason for that might be that criterion CC is based on correlation calculation, and such an approach is very resistant to noise and other signal fluctuations. Criterion RC includes a very symmetric and regular curve: it uses both the real and imaginary part of the reconstructed complex field, and this means that it takes benefit from both amplitude and phase encoded in the real and imaginary parts. The SPEC criterion is found to have the highest computational cost due to the need for calculating FFT. The SPEC is a relatively robust criterion for amplitude and phase images, although it requires FFT computation. Note also that the peak or valley is not very sensitive to the filtering parameters (filtering radius), which may vary over a wide range of values. Criteria that are able to produce a regular curve with a distinguishable peak are of major interest. This point is important, because this means that for criteria exhibiting a regular curve, this curve can be fitted by an analytical mathematical function. This provides a considerable advantage compared to other criteria because, using such modelling, the distance scan would not require so many distance computations to determine the peak (or valley) and to determine the optimal distance using least square fitting, for example. Considering this point, CC and RC criteria are certainly the more adapted to such an approach.

Table 2. Average Computation Time of Criteria

Criteria	Number of Reconstructed Planes	Average Processing Time (ms)
GRAX	80	0.124
GRAY	80	0.107
GRA	80	0.093
LAP	80	0.134
LAPMAX	80	0.084
VAR	80	0.439
SPEC	80	4.300
Md	80	0.075
ENTR	80	0.075
TC	80	0.070
GI	80	0.125
RC	80	0.133
CC	80	1.100

7. CONCLUSION

This paper proposes a quality assessment of focusing criteria for particle imaging in digital off-axis holography. A set of 13 criteria was investigated. Simulations were carried out to generate digital holograms of opaque and phase particles by taking into account some alias and noise. Refocus criteria were applied to both amplitude image and phase image obtained from off-axis digital holographic simulations. This was also conducted in the same way by considering experiments with a noncalibrated opaque particle. The computational costs were estimated for each criterion. In order to briefly summarize the results obtained within this study, it was found that the most robust criteria are the CC [17–19] and the RC [20]. Such criteria are able to systematically produce a regular curve with a peak or a valley at the correct focus distance; for this reason they are of major interest. Such a regular curve could be fitted by analytical equation, and this modelling would not require too many distance computations to determine the peak (or valley) and to determine the optimal distance by

least square fitting with a reduced set of reconstructed images. Future work will consider such an approach for high-speed refocusing in digital holographic particle imaging.

Funding. Ministère de l'Enseignement et de la Recherche Scientifique, Algérie (381/PNE/ENS/FRANCE/2015-2016).

REFERENCES

1. J. W. Goodman and R. W. Lawrence, "Digital image formation from electronically detected holograms," Appl. Phys. Lett. **11**, 77–79 (1967).
2. T. Kreis, *Handbook of Holographic Interferometry: Optical and Digital Methods* (Wiley, 2004).
3. T. C. Poon, *Digital Holography and Three-Dimensional Display: Principles and Applications* (Springer-Verlag, 2010).
4. P. Picart, *New Techniques in Digital Holography* (ISTE-Wiley, 2015).
5. J. Gillespie and R. A. King, "The use of self-entropy as a focus measure in digital holography," Pattern Recogn. Lett. **9**, 19–25 (1989).
6. Z. Ren, N. Chen, and E. Y. Lam, "Extended focused imaging and depth map reconstruction in optical scanning holography," Appl. Opt. **55**, 1040–1047 (2016).
7. L. Ma, H. Wang, Y. Li, and H. Jin, "Numerical reconstruction of digital holograms for three-dimensional shape measurement," J. Opt. A **6**, 396–400 (2004).
8. M. L. Tachiki, M. Itoh, and T. Yatagai, "Simultaneous depth determination of multiple objects by focus analysis in digital holography," Appl. Opt. **47**, D144–D153 (2008).
9. F. Dubois, C. Schockaert, N. Callens, and C. Yourassowsky, "Focus plane detection criteria in digital holography microscopy by amplitude analysis," Opt. Express **14**, 5895–5908 (2006).
10. M. Antkowiak, N. Callens, C. Yourassowsky, and F. Dubois, "Extended focused imaging of a microparticle field with digital holographic microscopy," Opt. Lett. **33**, 1626–1628 (2008).
11. C. Trujillo and J. Garcia-Sucerquia, "Automatic method for focusing biological specimens in digital lensless holographic microscopy," Opt. Lett. **39**, 2569–2572 (2014).
12. C. Trujillo and J. Garcia-Sucerquia, "Comparative analysis of the modified enclosed energy metric for self-focusing holograms from digital lensless holographic microscopy," Appl. Opt. **54**, 5102–5108 (2015).
13. J. F. Restrepo and J. Garcia-Sucerquia, "Automatic three-dimensional tracking of particles with high-numerical-aperture digital lensless holographic microscopy," Opt. Lett. **37**, 752–754 (2012).
14. F. C. Groen, I. T. Young, and G. Ligthart, "A comparison of different focus functions for use in autofocus algorithms," Cytometry **6**, 81–91 (1985).
15. P. Langehanenberg, B. Kemper, B. Dirksen, D. Dirksen, and G. von Bally, "Autofocusing in digital holographic phase contrast microscopy on pure phase objects for live cell imaging," Appl. Opt. **47**, D176–D182 (2008).
16. F. Toy, S. Richard, J. Kühn, A. Franco-Obregón, M. Egli, and C. Depeursinge, "Enhanced robustness digital holographic microscopy for demanding environment of space biology," Biomed. Opt. Express **3**, 313–326 (2012).
17. Y. Yang, B.-S. Kang, and Y.-J. Choo, "Application of the correlation coefficient method for determination of the focal plane to digital particle holography," Appl. Opt. **47**, 817–824 (2008).
18. Y. Yang and B.-S. Kang, "Experimental validation for the determination of particle positions by the correlation coefficient method in digital particle holography," Appl. Opt. **47**, 5953–5960 (2008).
19. J. Liu, X. Song, R. Han, and H. Wang, "Autofocus method in digital holographic microscopy," Proc. SPIE **7283**, 72833Q (2009).
20. S. Grare, S. Coëtmellec, D. Allano, G. Gréhan, M. Brunel, and D. Lebrun, "Dual-wavelength digital holography for 3D particle image velocimetry," J. Eur. Opt. Soc. **10**, 15009 (2015).
21. P. Memmolo, C. Distante, M. Paturzo, A. Finizio, P. Ferraro, and B. Javidi, "Automatic focusing in digital holography and its application to stretched holograms," Opt. Lett. **36**, 1945–1947 (2011).
22. P. Memmolo, M. Paturzo, B. Javidi, P. A. Netti, and P. Ferraro, "Refocusing criterion via sparsity measurements in digital holography," Opt. Lett. **39**, 4719–4722 (2014).
23. D. Zonoobi, A. A. Kassim, and Y. V. Venkatesh, "Gini Index as sparsity measure for signal reconstruction from compressive samples," IEEE J. Sel. Top. Signal Process. **5**, 927–932 (2011).
24. J. Dohet-Eraly, C. Yourassowsky, and F. Dubois, "Fast numerical autofocus of multispectral complex fields in digital holographic microscopy with a criterion based on the phase in the Fourier domain," Opt. Lett. **41**, 4071–4074 (2016).
25. L. Xu, M. Mater, and J. Ni, "Focus detection criterion for refocusing in multi-wavelength digital holography," Opt. Express **19**, 14779–14793 (2011).
26. M. Liebling and M. Unser, "Autofocus for digital Fresnel holograms by use of a Fresnelet-sparsity criterion," J. Opt. Soc. Am. A **21**, 2424–2430 (2004).
27. E. S. Fonseca, P. T. Fiadeiro, M. Pereira, and A. Pinheirao, "Comparative analysis of autofocus functions in digital in-line phase-shifting holography," Appl. Opt. **55**, 7663–7674 (2016).
28. P. Picart and P. Tankam, "Analysis and adaptation of convolution algorithms to reconstruct extended objects in digital holography," Appl. Opt. **52**, A240–A253 (2013).